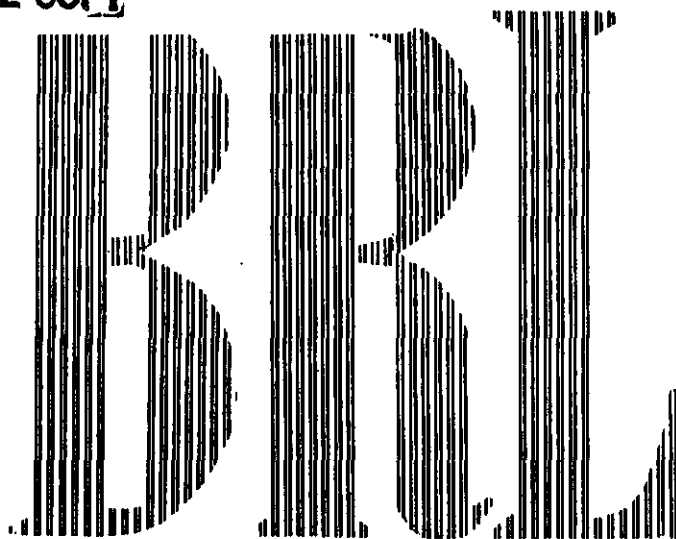
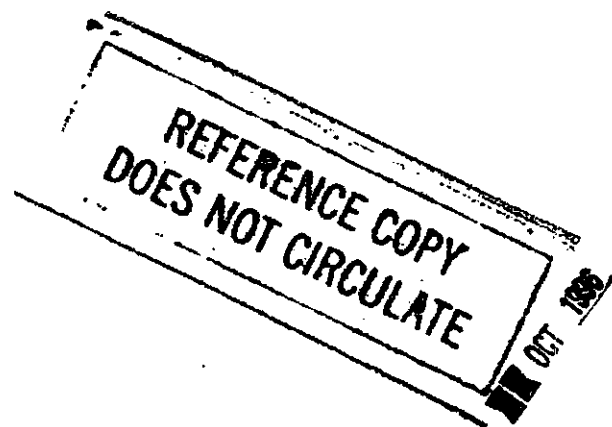


**REFERENCE COPY**



**TECHNICAL NOTE No. 841**

**AFSWP No. 722**



# **Diffraction of Step Shocks Through a Double Slit**

**GEORGE COULTER**

**JAMES ALLEN**

**TECHNICAL LIBRARY  
AMXBR-LB (Bldg. 305)  
ABERDEEN PROVING GROUND, MD. 21005**

**DEPARTMENT OF THE ARMY PROJECT No. 503-04-002  
ORDNANCE RESEARCH AND DEVELOPMENT PROJECT No. TB3-0112J**

The Ballistic Research Laboratories Technical Note is designed for use within the laboratories or for issuing available information, when the occasion demands speed.

The contents of this paper are of the nature of advance information and may be extended or otherwise revised.

**BALLISTIC RESEARCH LABORATORIES**



**ABERDEEN PROVING GROUND, MARYLAND**

10804

BALLISTIC RESEARCH LABORATORIES

TECHNICAL NOTE NO. 841

AFSMP NO. 722

JANUARY 1954

DIFFRACTION OF STEP SHOCKS THROUGH A DOUBLE SLIT

George Coulter

James Allen

TECHNICAL LIBRARY  
AMXBR-LB (Bldg. 305)  
ABERDEEN PROVING GROUND, MD. 21005

Department of the Army Project No. 503-04-002  
Ordnance Research and Development Project No. TB3-0112J

Funds for this work were supported by the  
Armed Forces Special Weapons Project.

ABERDEEN PROVING GROUND, MARYLAND

BALLISTIC RESEARCH LABORATORIES

TECHNICAL NOTE NO. 841

AFSWP NO. 722

JANUARY 1954

GCoulter/ow  
Aberdeen Proving Ground, Md.  
January 1954

DIFFRACTION OF STEP SHOCKS THROUGH A DOUBLE SLIT

ABSTRACT

An experiment, using a four and one-half inch shock tube, is described, showing the results obtained when a step shock wave is allowed to be diffracted by a wall with two  $1/8 \times 1/8$  inch slits spaced one inch apart. The effects of the slits in the wall were made two-dimensional by letting the length of the slits extend across the vertical diameter of the tube.

Spark shadowgraphs of the resulting phenomena, after the shock wave has been diffracted through the slits, are shown. Triple point measurements taken from shadowgraphs are presented in graphical form for five different peak pressures incident upon the model. The pressure values are the calculated values of the shock pressures before diffraction.

## INTRODUCTION

Work on the diffraction of a shock wave through a single slit of varying width was published by G. Uhlenbeck of the University of Michigan in 1950. His work showed a diffracted front which became flatter as the slit width increased. Further work was reported at the Salt Lake City (1951) meeting of the Fluid Dynamics Division of the American Physical Society by Henry Alberts of the Ballistic Research Lab.. In his work, a wall with a single slit size was used with varying pressure to obtain the various diffraction phenomena. In this case the shape of the wave fronts was determined to be cylindrical. During the same session of the Society, Elder and de Haas of the Johns Hopkins Applied Physics Laboratory described the formation of a vortex ring at the end of a shock tube. The decay of pressure behind the shock front appeared to be of an exponential form.

The present paper extends the work of the previous authors to the case of two equal slits through which step shocks are allowed to pass. The shocks were all of the air to air variety with the expansion chamber at atmospheric pressure.

## DESCRIPTION OF APPARATUS

Figure 1 shows the 4 1/2 inch diameter shock tube used in the experiment. The numbers label the various parts. Item (1) in Fig. 1 is the high pressure compression chamber. A cellophane diaphragm separates the compression chamber, which is filled with compressed air, from the expansion chamber. The air pressure is varied to obtain the desired excess peak pressure ( $P_s$ ) after the diaphragm is ruptured. The shock remains at a roughly constant pressure for a duration of between two to five milliseconds, if no reflection or diffraction occurs.

Item (2) in Fig. 1 shows the position of the two Schlieren light screens and photo-multiplier combinations which were triggered when the shock wave diffracted the beams of light onto the photocells. The pulses from the photocells started and stopped a 1.6 megacycle counter for shock velocity calculation. The second pulse, which was the stop pulse for counter 1, was also used to start a second 1.6 megacycle counter which was in turn stopped by the induced pulse from the firing of the spark gap. The pulse from the second light screen also triggered a delay unit (6) which allowed the shock wave to progress into the field of the photographic windows (3) before triggering the spark gap (5) for the shadow picture exposure on high contrast film (4). Item (7) indicates the high voltage supply to the spark gap. The gap was operated at approximately 9,000 volts.

A quartz collimating lens was used to make the light nearly parallel in order to eliminate as much parallax and resultant inaccuracy in the image as possible.

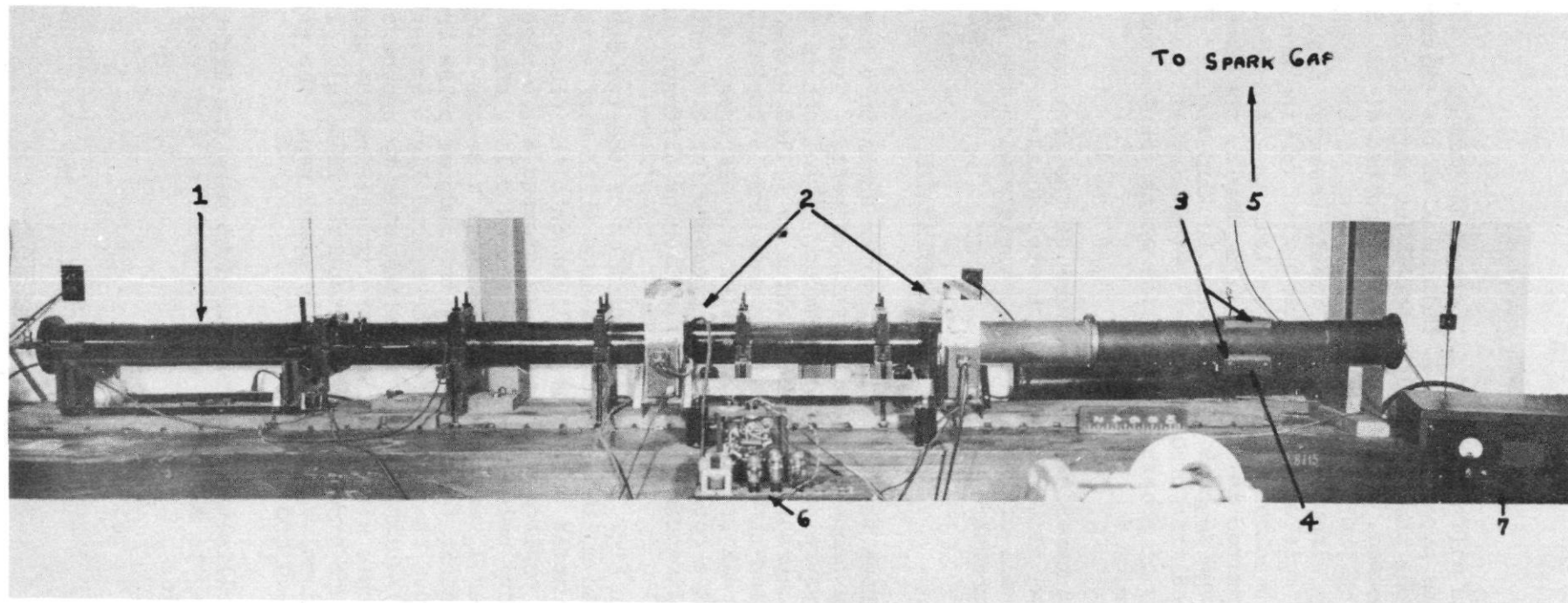


FIGURE 1. 4-1/2" Shock Tube, Aberdeen Proving Ground, Maryland.

## DESCRIPTION OF THE WALL USED

A diagram of the wall used in the experiment is shown in Fig. 2. All data measurements made on the photographs were made from the point (0,0) at the center of the upstream side of the wall.

It should be emphasized that the incident pressure ( $P_s$ ) is the accurate pressure calculated from shock velocity measurement before reflection and diffraction occur, but that it does not define the pressure after the stated phenomena take place. The shadowgraphs which are shown were taken as the shock fronts traveled along in the region of the viewing windows after diffraction. Striations in the pictures are apparent, due to the use of ordinary plate glass for the windows.

## DESCRIPTION OF THE SHADOWGRAPHS

Figures 3-13 are shadowgraphs of eleven separate shots. In the absence of a multiple spark, the use of several shots at constant pressure is an approach to a time sequence for a single shot. The pressure incident at the front of the model is about  $5.5 \text{ lbs./in.}^2 \pm 2\%$  maximum scatter. This error in pressure will cause almost no change in the phenomena after diffraction. The distance coordinates will suffer a slight inaccuracy ( $\pm .01 \text{ in.}$ ) if the pressure has a deviation maximum of  $\pm 2\%$  from the average for the discrete shots of a 'constant' pressure series.

Figure 3 shows the shock approaching from the left somewhat over half of the distance through the slit. The shock wave to the left of the slits has been reflected.

Figures 4 and 5 show the growth of the diffracted cylindrical fronts expanding from the two slits. The vortices on both the inside and outside edges of the slits, for the most part, have a circular appearance devoid of the formation of density layers as yet.

At the time of Fig. 6, a group of shocks is forming inside the slits, due to a choking by the boundary layer at the slit walls thereby creating, in effect, a de Laval nozzle, or miniature wind tunnel. If the flow conditions are correct, then shocks may form in order to satisfy the conservation equations. The interaction at the intersection of the two cylindrical fronts will be examined more closely later.

Figures 7 and 8 show the interaction of the cylindrical fronts with the vortices. The weak waves in Fig. 8, which appear to come from the vortices, are the results of these interactions, shown in clearer detail in Figs. 14, 15, and 16 to be discussed later.

Figure 9 shows a Mach stem now beginning to grow at  $A' - A$ . Above the upper vortex, a weak wave front is noticeable due to the reflection of the diffracted cylindrical wave as its end moves along the wall of the tube.

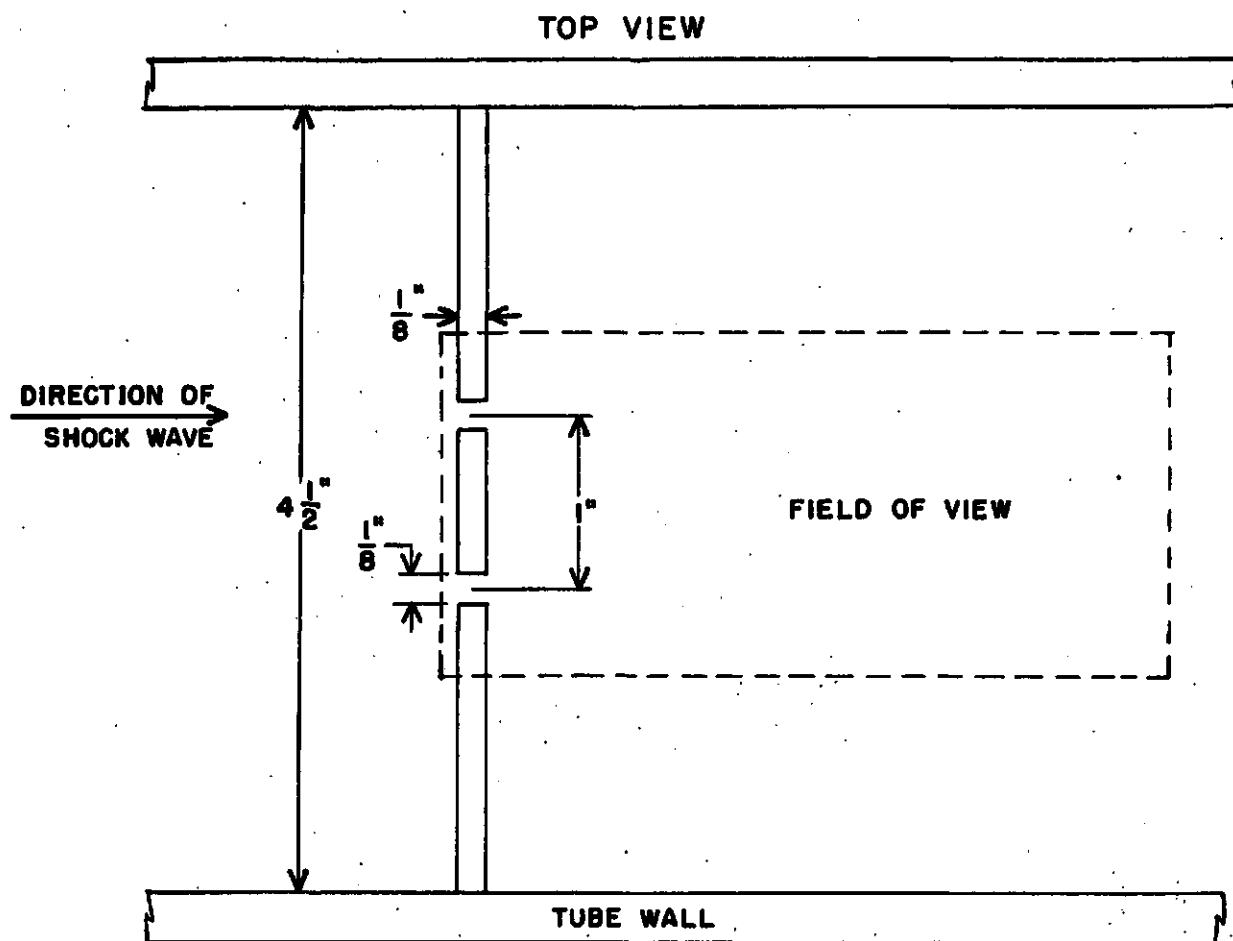


FIGURE 2  
 DIAGRAM OF WALL IN SHOCK TUBE

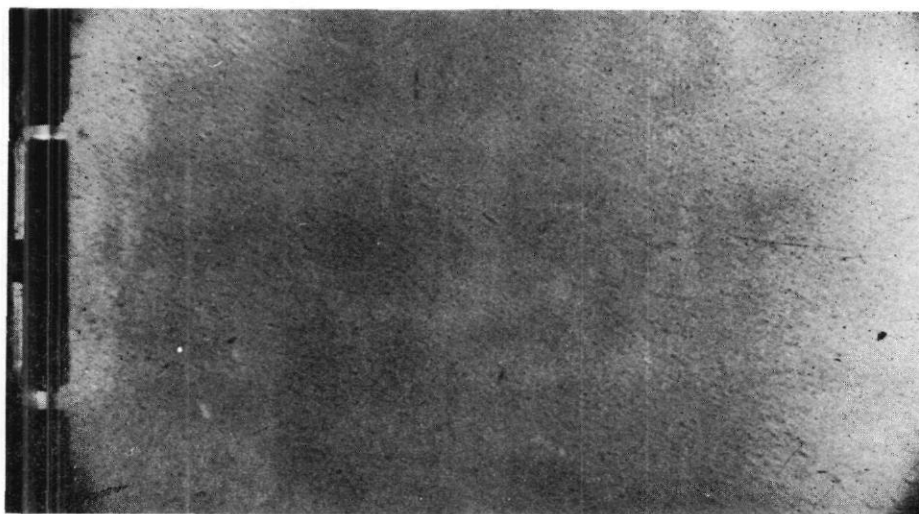


FIGURE 3

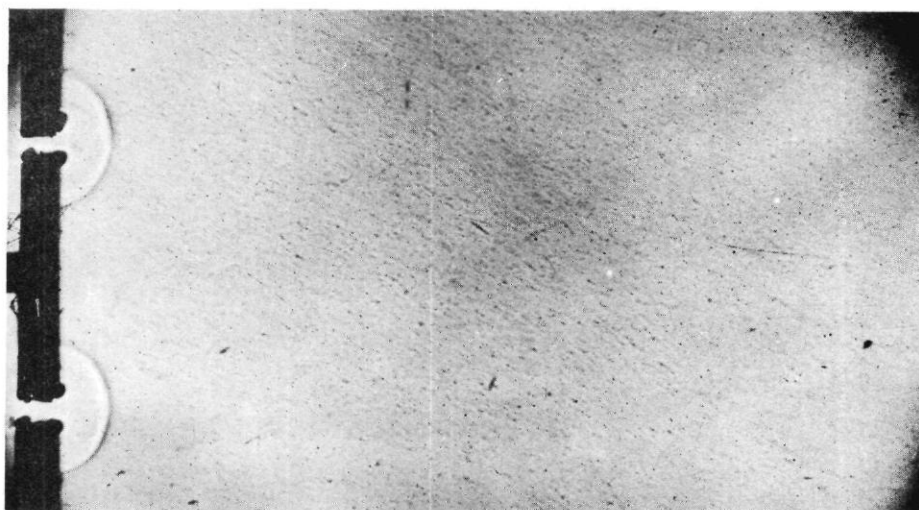


FIGURE 4



FIGURE 5



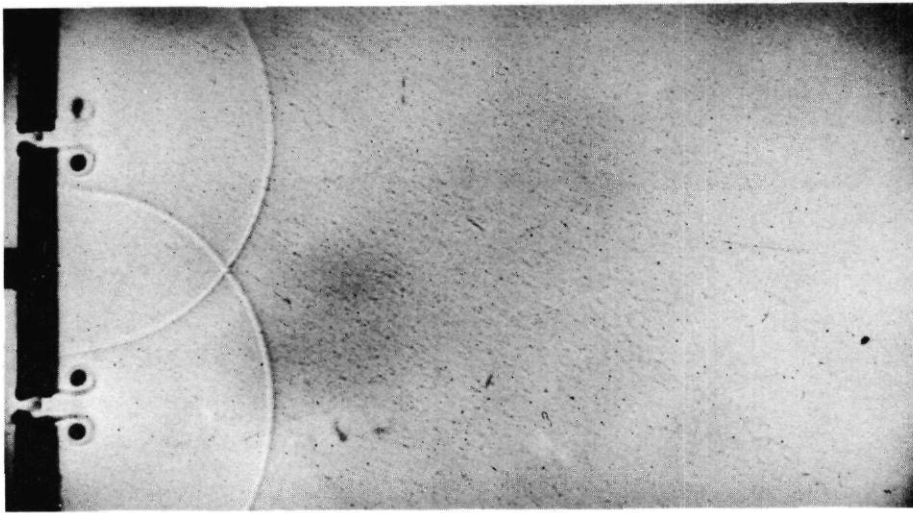


FIGURE 6

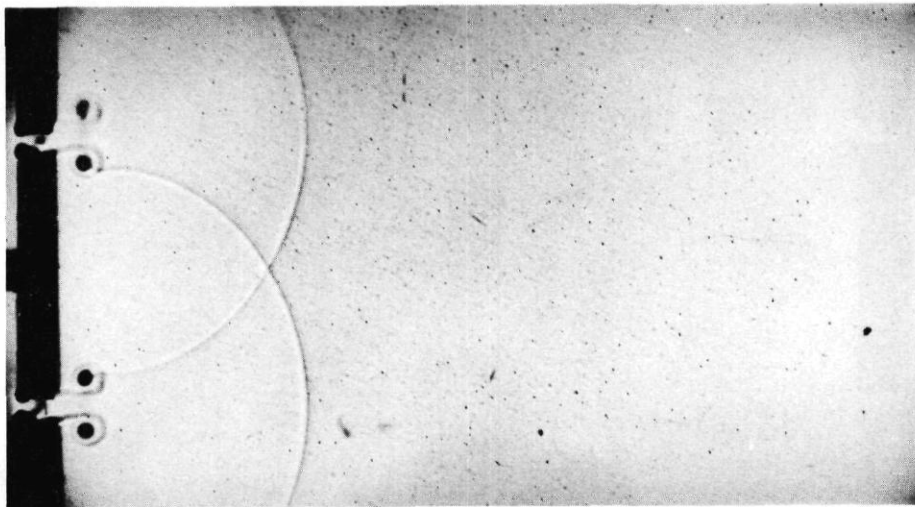


FIGURE 7

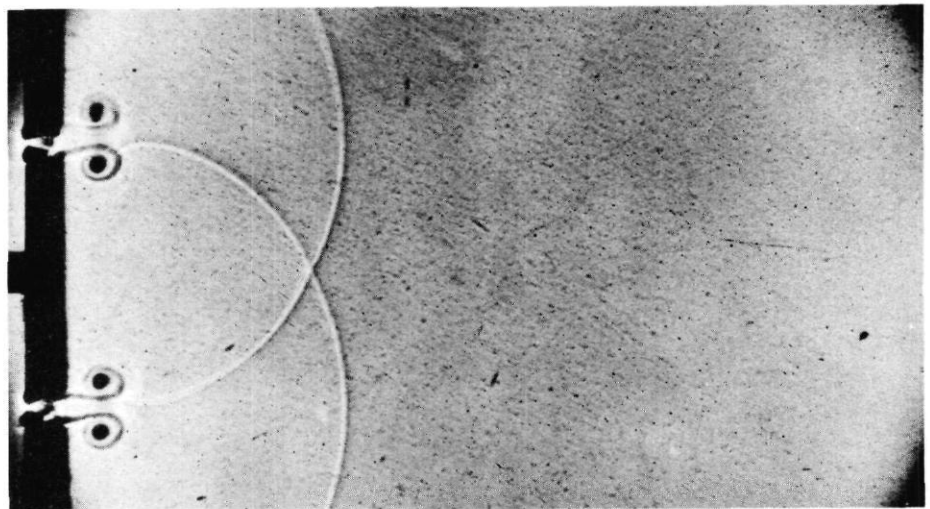


FIGURE 8

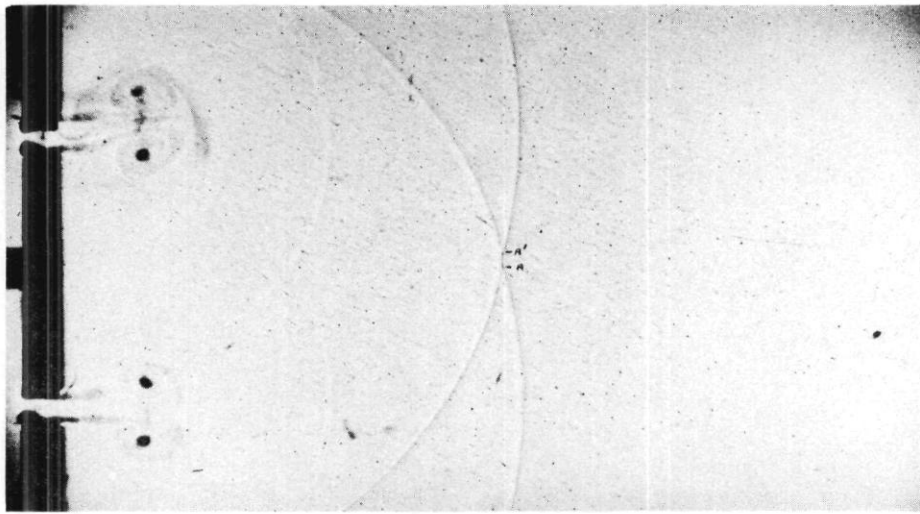


FIGURE 9

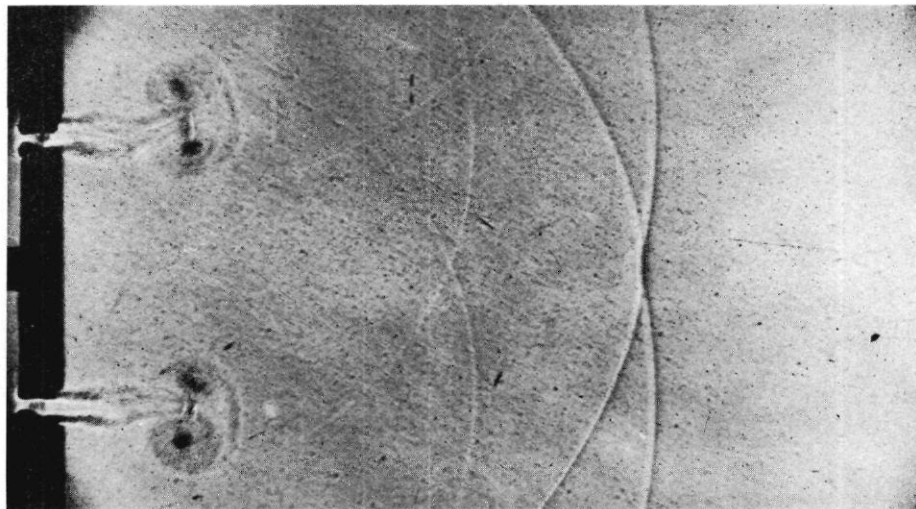


FIGURE 10

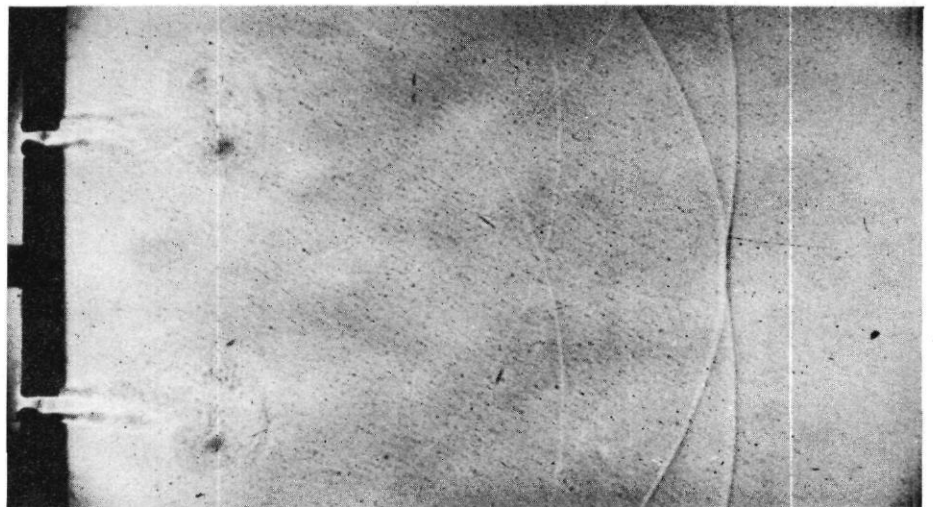


FIGURE 11



FIGURE 12



FIGURE 13

Figures 10, 11, and 12 show the continuation of the Mach stem growth. Finally, Fig. 13 shows only turbulence from the vortices with all signs of the interacting fronts gone.

Figures 14, 15, and 16 are presented to aid in acquiring a clearer understanding of the cylindrical front interacting with the vortex. Figures 14 and 15 are offered as proof that the cylindrical wave is furnishing the interacting components for the generation of the weak waves near the vortices, rather than, perhaps, some internal phenomena of the vortex itself. The time and pressure values are approximately the same for both of the figures. In Fig. 15 one slit has been blocked off so that only one diffracted wave is evident. There is no indication of any interaction occurring in the vortex region now that the diffracted wave from the second slit is no longer present. This is the basis for the contention that the interaction between the respective vortices and the diffracted waves accounts for the phenomena detected in Fig. 14. The interaction to be discussed is that centered around the bottom slit. In Fig. 14 the cylindrical fronts from the two slits have interacted to cause the small Mach stem  $A' - A$ . The diffracted front  $D^0$  travels downward until it hits vortex I. When the collision occurs, two things happen. A portion of the wave is reflected to give  $D^0$ ; another portion of the wave is transmitted which becomes diffracted and rotated in vortex I, expands as the jet stream strikes it, and is 'blown' out to become  $D_+$ . Many additional photographs furnish corroborative evidence to verify this concept. Another portion of the wave is transmitted through both vortices to give  $D_+$ . A part is also reflected back from the jet stream to produce the wave  $R$  in Fig. 16. When vortex II is hit by  $D_+$ ,  $D^0$  is reflected from this vortex and a part continues through; but, no wave has been rotated around and 'blown' out in front as in the case of vortex I. See also Fig. 16-a. Two conditions are suggested which may be able to account for the absence of the interaction of the second vortex. The first condition is that the vortices are now slowing down, thus causing less of a rotational interaction. The second condition is that there is a lack of a jet stream on the further side of vortex II. Therefore, no 'blowing' effect is possible. Without this 'blowing' process, apparently, no wave is produced to expand outwardly from the second vortex.

Figure 16 has two other discontinuities which are interesting. These are clearly demonstrated for the greatest pressure ( $P_s = 12.7$  lbs/in.<sup>2</sup>). The first is that the contact discontinuity, or slip stream, which appears at C is necessary in order to satisfy the conservation equations of a three shock configuration. The second wave is labeled B. It appears because the model does not touch either of the viewing windows (in order to prevent scratching of the windows). This setup allows a shock to pass over and under the model into the viewing section where it is photographed as a separate shock wave.

#### DISCUSSION OF THE TRIPLE POINT GROWTH

Five sets of photographs were taken at different constant incident pressures:  $P_s = 3.2, 4.1, 5.4, 8.5,$  and  $12.7$  lbs/in.<sup>2</sup>. Several shots were taken at positions similar to those in the shadowgraphs previously

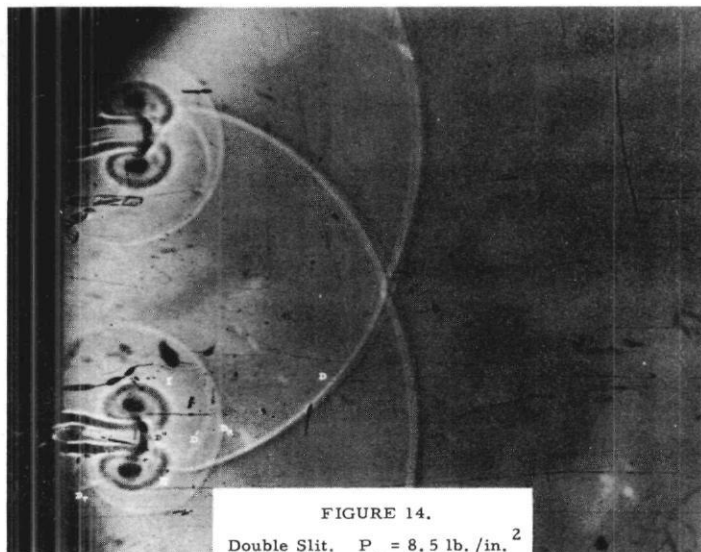


FIGURE 14.  
Double Slit.  $P_g = 8.5 \text{ lb./in.}^2$

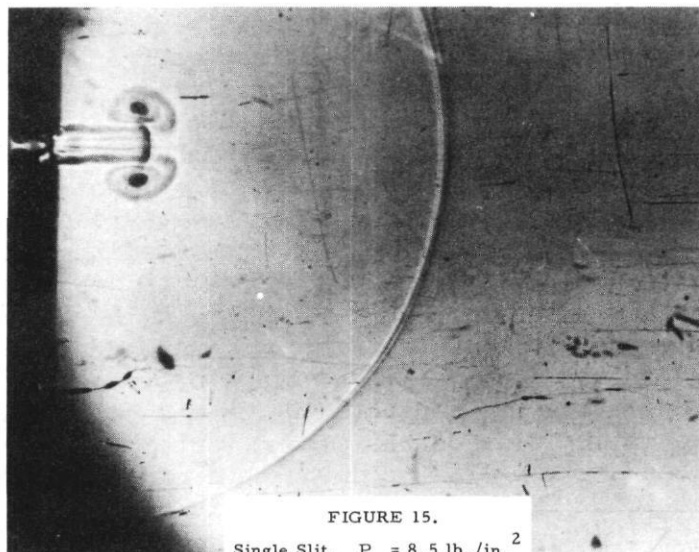


FIGURE 15.  
Single Slit.  $P_g = 8.5 \text{ lb./in.}^2$

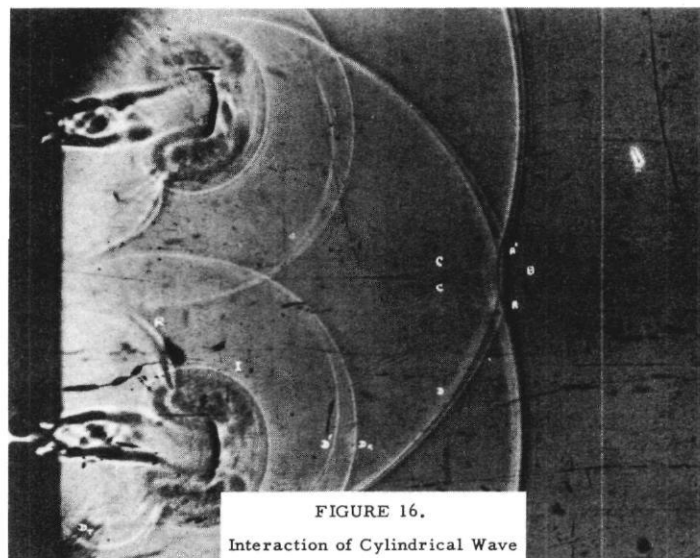


FIGURE 16.  
Interaction of Cylindrical Wave  
Front With Vortex.

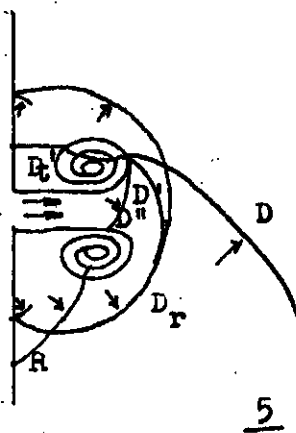
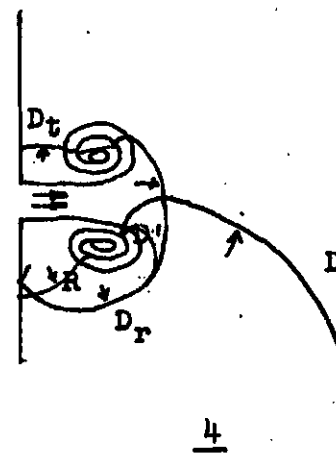
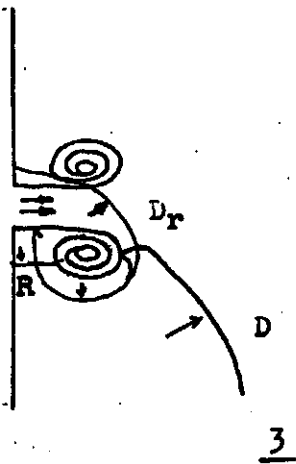
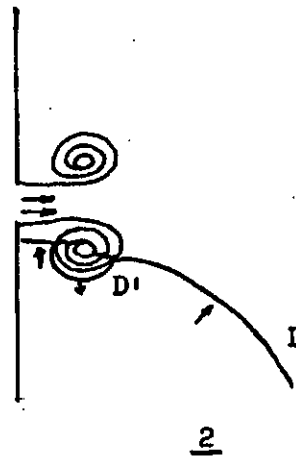
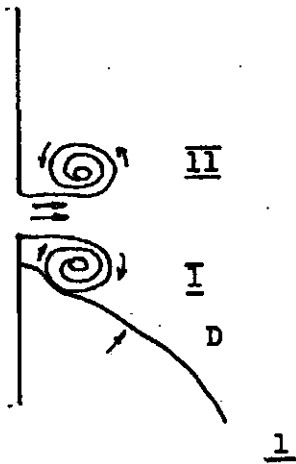


Figure 16 A  
Sketch of Cylindrical Wave Front  
Interacting With  
Vortex



shown. The X-Y coordinates of the triple point A<sup>1</sup> for these photographs are plotted in Fig. 17 for each of the constant pressure series.

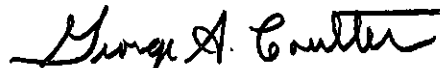
It can be seen that each of these series tends to some value of X when Y=0. This point (D<sub>0</sub>) corresponds to the value for which regular reflection ceases and Mach reflection begins for that particular pressure ratio across the shock front. Unfortunately, since the least reading of the experimental measurements involved is approximately 0.01 in., there is uncertainty as to where, exactly, the actual value of X=D<sub>0</sub> falls. For the curve of P<sub>s</sub>=12.7 lbs/in.<sup>2</sup>, this point is probably at X = 70 units. This is not immediately obvious from an investigation of the curve. However, a possible error of approximately 0.02 inch in reading the photographs leads to an inherently high figure for D<sub>0</sub> as read. At this value of D<sub>0</sub>= 70, extreme = 49°.

Additional information is obtained if the growth of the Mach stem is compared for a constant X distance with P<sub>s</sub> allowed to vary. Figure 18 demonstrates this photographically and Fig. 19 shows the data plotted with the Y coordinate as a function of P<sub>s</sub> for the constant X coordinate equal to 307 (+ 1) units (as measured from the shadowgraphs).

#### CONCLUSION

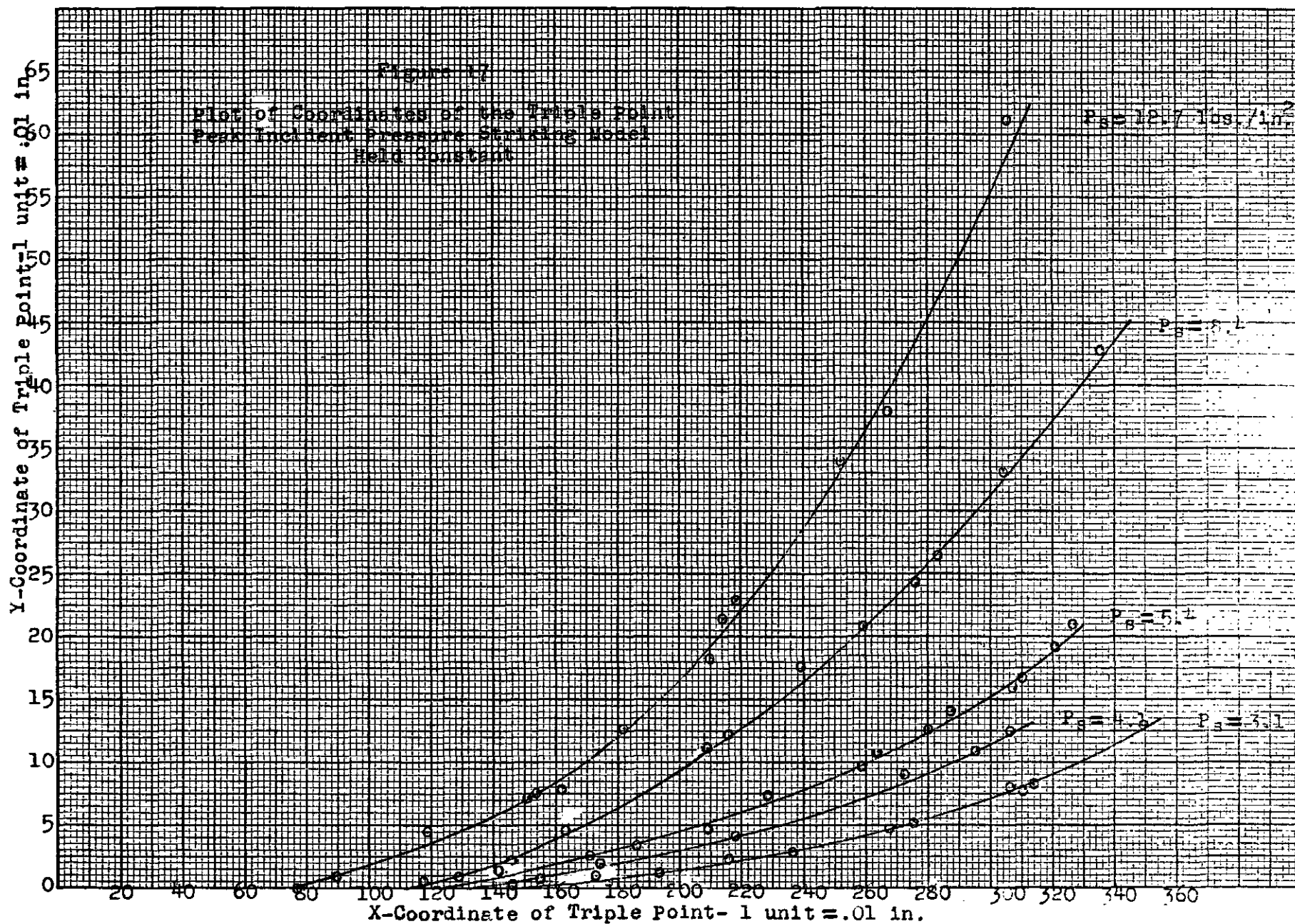
Shadowgraphs have been presented showing the interaction between two cylindrical shock fronts produced by the diffraction of a step shock through two small slits. A plot of the growth of the Mach stem versus distance was made at several shock pressure levels. However, sufficiently accurate peak pressure measurements of the Mach front could not be made to enable scaling and theoretical correlation of the results. Perhaps development of the multiple-spark shadowgraph system will make possible velocity measurements of the required degree of precision.

The brief study of the interaction of a wave front and a vortex presents, together with supporting shadowgraphs, a cause and effect theory of a very complicated phenomenon.



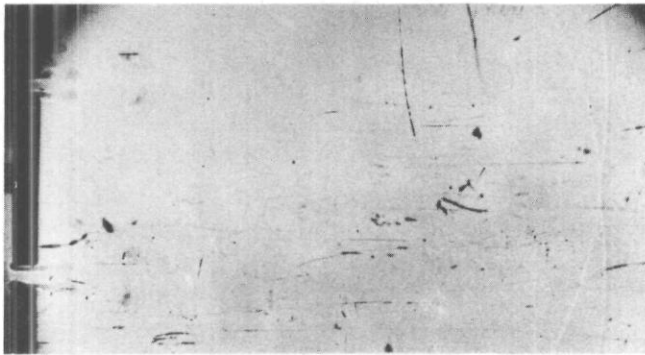
GEORGE COULTER

  
JAMES ALLEN

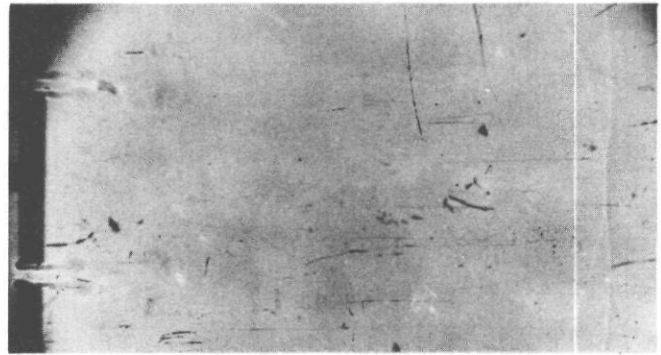




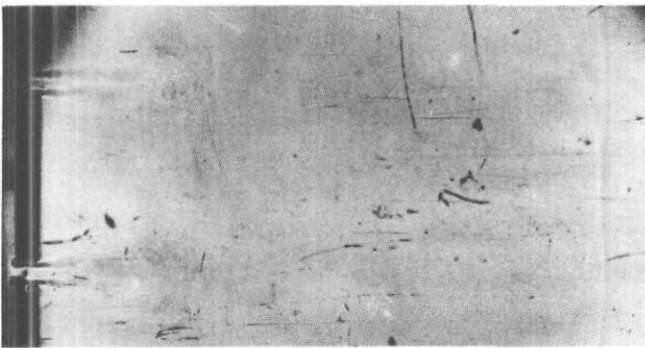
X-Coordinate Held Constant  
( $x = 3.07$  ins.)



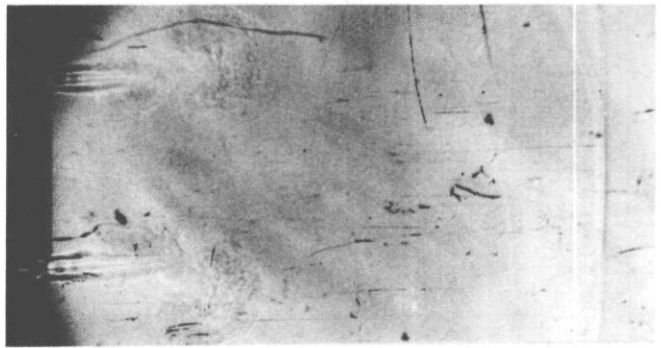
$$P_s = 3.20 \text{ lb./in.}^2 \quad Y = .08 \text{ in.}$$



$$P_s = 4.17 \text{ lb./in.}^2 \quad Y = .12 \text{ in.}$$



$$P_s = 5.52 \text{ lb./in.}^2 \quad Y = .19 \text{ in.}$$

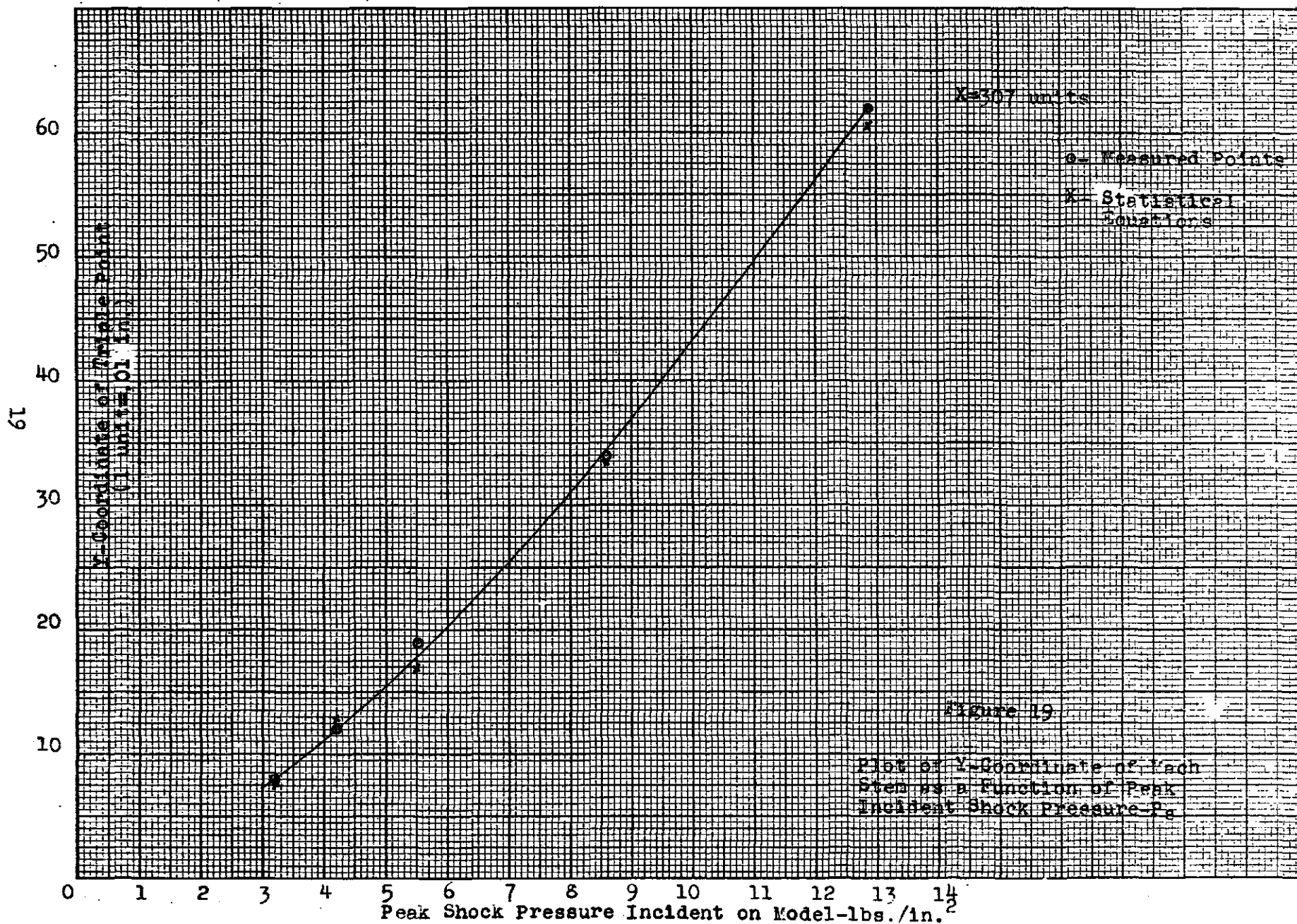


$$P_s = 8.58 \text{ lb./in.}^2 \quad Y = .34 \text{ in.}$$



$$P_s = 12.87 \text{ lb./in.}^2 \quad Y = .57 \text{ in.}$$

FIGURE 18. Shadowgraphs Showing Growth of Mach Stem As a Function of  $P_s$ .



# DISTRIBUTION LIST

<u>No. of Copies</u>	<u>Organization</u>	<u>No. of Copies</u>	<u>Organization</u>
4	Chief of Ordnance Department of the Army Washington 25, D. C. Attn: ORDTB - Bal Sec	1	Director of Intelligence United States Air Force Washington 25, D. C. Attn: Lt. Col. John W. Ault Deputy Director for Targets Physical Vulnerability Branch
4	Chief, Bureau of Ordnance Department of the Navy Washington 25, D. C. Attn: Re3	1	Commander Air Research and Development Command P. O. Box 1395 Baltimore 3, Maryland Attn: Lt. Col. D. L. Crowson
2	Commander Naval Ordnance Laboratory White Oak Silver Spring 19, Maryland Attn: Explosives Division	1	Commanding Officer Air Force Cambridge Research Laboratory 230 Albany Street Cambridge, Massachusetts Attn: FRHS-1, Geophysical Research Library
1	Commander Naval Ordnance Test Station Inyokern P. O. China Lake, California Attn: Technical Library	1	Commander Air Materiel Command Wright-Patterson Air Force Base, Ohio Attn: MCAIDS
1	Director Naval Research Laboratory Anacostia Station Washington 20, D. C.	1	Diamond Ordnance Fuze Laboratories Connecticut Avenue at Van Ness Street, N.W. Washington 25, D. C. Attn: Mr. Fred Harris, Division 20
1	Chief, Bureau of Yards and Docks Department of the Navy Washington 25, D. C. Attn: Code P-300	1	Director David Taylor Model Basin Washington 7, D. C. Attn: Structural Mechanics Division
1	Officer in Charge Naval Civil Engineering Research & Evaluation Laboratory Naval Station Port Hueneme, California	5	Armed Forces Special Weapons Project P. O. Box 2610 Washington 25, D. C. Attn: Blast Branch
1	Deputy Chief of Staff Development Research & Development Directorate United States Air Force Washington 25, D. C. Attn: Chief, Research Division		

# DISTRIBUTION LIST

<u>No. of Copies</u>	<u>Organization</u>	<u>No. of Copies</u>	<u>Organization</u>
1	Chief of Engineers Department of the Army Washington 25, D. C. Attn: Mr. M. D. Kirkpatrick	1	Broadview Research & Development P. O. Box 1093 Burlingame, California Attn: Dr. Richard I. Condit
1	Commanding General Technical Command Army Chemical Center, Maryland	1	Dr. John M. Richardson Institute of Industrial Research University of Denver Denver 10, Colorado
1	Los Alamos Scientific Laboratory P. O. Box 1663 Los Alamos, New Mexico Attn: Dr. Fred Reines	1	Dr. S. J. Fraenkel Division of Engineering Mechanics Armour Research Foundation Chicago 16, Illinois
5	Director Armed Services Technical Information Agency Documents Service Center Dayton 2, Ohio Attn: DSC - SA	1	Dr. R. J. Hansen Massachusetts Institute of Technology Cambridge 39, Massachusetts
1	Director, Project RAND Department of the Air Force 1700 Main Street Santa Monica, California Attn: Mr. Marc Peter	1	Dr. N. M. Newmark 111 Talbot Laboratory University of Illinois Urbana, Illinois
1	Applied Physics Laboratory 8621 Georgia Avenue Silver Spring, Maryland	1	Dr. Otto LaPorte Engineering Research Institute University of Michigan Ann Arbor, Michigan
2	Sandia Corporation P. O. Box 5800 Albuquerque, New Mexico Attn: Physics Div. - Dr. E. Cox Blast Model Studies Div. Dr. J. Shreve	1	Dr. Walker Bleakney Princeton University Princeton, New Jersey
		1	Dr. J. Kirkwood Department of Chemistry Yale University New Haven, Connecticut